Vibrational resolved partial cross sections and asymmetry parameters for nitrogen K-shell photoionization of the N2O molecule

著者	Lucchese R. R., Soderstrom J., Tanaka T., Hoshino M., Kitajima M., Tanaka H., Fanis A. De, Rubensson J.-E., Ueda K.
journal or publication title	Physical Review. A
volume	76
number	1
page range	012506
year	2007
URL	http://hdl.handle.net/10097/53616

doi: 10.1103/PhysRevA.76.012506

Vibrationally resolved partial cross sections and asymmetry parameters for nitrogen *K*-shell photoionization of the N_2O molecule

R. R. Lucchese*
Institute of Multidisciplinary Research for Advanced Materials, Tohoku University, Sendai 980-8577, Japan and Department of Chemistry, Texas A&M University, College Station, Texas 77843-3255, USA

J. Söderström
Institute of Multidisciplinary Research for Advanced Materials, Tohoku University, Sendai 980-8577, Japan and Department of Physics, Uppsala University, P.O. Box 530, SE-751 21 Uppsala, Sweden

T. Tanaka, M. Hoshino, M. Kitajima,† and H. Tanaka
Department of Physics, Sophia University, Tokyo 102-8554, Japan

A. De Fanis
SPring-8/JASRI, Koto 1-1, Sayo-gun, Hyogo 679-5198, Japan

J.-E. Rubensson‡
Department of Physics, Uppsala University, P.O. Box 530, SE-751 21 Uppsala, Sweden

K. Ueda
Institute of Multidisciplinary Research for Advanced Materials, Tohoku University, Sendai 980-8577, Japan
(Received 30 April 2007; published 17 July 2007)

We have measured the vibrationally resolved partial cross sections $\sigma_{(v_1',v_2',v_3')}$ and asymmetry parameters $\beta_{(v_1',v_2',v_3')}$ for N_c and N_t *K*-shell photoionization of the N_2O molecule in the σ^* shape resonance region above the N_t and N_c *K*-shell ionization thresholds. N_c *K*-shell photoionization of the N_2O molecule predominantly causes the excitation of the quasisymmetric vibrations (v_1'), whereas N_t *K*-shell photoionization causes both quasisymmetric and quasiantisymmetric vibrations (v_1' and v_3') to be excited. The shape resonance energy in the N_c *K*-shell photoionization increases with an increase in v_1'. The $\beta_{(v_1',0,0)}$ curves for the N_c *K*-shell photoionization exhibit maxima at energies close to the shape resonance energies for the individual values of v_1'. The shape resonance energy in the N_t *K*-shell photoionization decreases with an increase in v_1' and slightly increases with an increase in v_3'. The $\beta_{(v_1',0,0)}$ curves show a significant state dependence in the region of the shape resonance, with the curves shifting to lower energy as v_1' increases. The vibrational state dependence of the cross sections $\sigma_{(v_1',v_2',v_3')}$ and asymmetry parameters $\beta_{(v_1',v_2',v_3')}$ are well reproduced by the theoretical calculations using the multichannel Schwinger configuration interaction (MCSCI) method, including both the N_c and N_t ion states.

DOI: 10.1103/PhysRevA.76.012506 PACS number(s): 33.60.Fy, 33.20.Rm, 33.70.Ca

I. INTRODUCTION

Shape resonances, which are described as a temporal trapping of the photoelectron by the molecular potential box, are the most intriguing features in molecular photoionization [1]. Some decades ago Dehmer and Dill [2] predicted that the shape resonance energy depends on the vibrational levels of the remaining molecular ion. Some decades later, high-resolution soft x-ray photoelectron spectroscopic studies revealed that the spectral and angular distributions for inner-shell photoemission from molecules in shape resonance regions depend on the final vibrational levels as predicted [3–11].

Among the best studied examples of this behavior is the inner-shell photoionization of carbon monoxide, CO: the shape resonance energy of the individual vibrational component v' in C 1*s* photoionization decreases with an increase in v' [3,4], whereas that in the O 1*s* photoionization increases with an increase in v' [6]. Mistrov *et al.* [6] interpreted these downward and upward shifts of the σ^* shape resonance to be a result of intramolecular interference of the scattered photoelectron waves in the CO molecule, where with increasing v', the effective C-O distance, $R_i(v')$, increases with an increase in v' for the C 1*s* ionized state and decreases with an increase in v', for the O 1*s* ionized states [6]. These v'-dependent shape resonance features were well reproduced by the calculations based on relaxed-core Hartree-Fock approximation [7]. Similar v' dependent shape resonances are also found in H_2CO [9], N_2 [10], and C_2H_2 [11].

*Corresponding author. lucchese@mail.chem.tamu.edu
†Present address: Department of Chemistry, Tokyo Institute of Technology, Tokyo 152-8551, Japan.
‡Present address: BESSY, Albert-Einstein-Strasse 15, 12489 Berlin, Germany.

Recently, vibrationally resolved partial cross sections σ and asymmetry parameters β were measured for carbon and oxygen K-shell photoionization of the CO_2 molecule [12,13]. The CO_2 molecule has four vibrational modes, symmetric $(v_1',0,0)$ and antisymmetric $(0,0,v_3')$ stretching modes, and a doubly degenerate bending mode $(0,v_2',0)$. The C $1s$ photoionization is accompanied by excitation of the symmetric stretching vibrations $(v_1',0,0)$ [14], whereas O $1s$ photoionization is accompanied by excitation of antisymmetric vibrations $(0,0,v_3')$ [14–17]. The shape resonance energy of the individual v_1' components in C K-shell photoionization decreases with an increase in v_1'. This tendency was well reproduced by the *ab initio* calculations employing the partially relaxed-core Hartree-Fock approximation [12]. The shape resonance energy of the individual v_3' component in O K-shell photoionization is, on the other hand, independent of v_3' [13]. Multiple scattering calculations within the vibrationally dependent fixed nuclei approach and the harmonic approximation well reproduced this v_3' independent nature of the shape resonance [13]. This v_3'-independent nature is a consequence of the fact that the antisymmetric vibrations do not change the size of the potential box responsible for the shape resonance.

In the present study, we extend our investigation, both experimentally and theoretically, to the vibrational state dependence of the shape resonances in the core-level photoionization of the dinitrogen oxide molecule, N_2O. N_2O is a linear molecule that has two nitrogen atoms in different sites, labeled as center (N_c) and terminal (N_t). The ground state electronic configuration [18] is

$$(1\sigma)^2(2\sigma)^2(3\sigma)^2(4\sigma)^2(5\sigma)^2(6\sigma)^2(1\pi)^4(7\sigma)^2(2\pi)^4 \times (3\pi)^0(8\sigma)^0(9\sigma)^0(^1\Sigma^+). \quad (1)$$

Here, 1σ, 2σ, and 3σ correspond to the O $1s$, N_c $1s$, and N_t $1s$ core orbitals, respectively. There are three unoccupied valence molecular orbitals 3π, 8σ, and 9σ. In the x-ray absorption spectrum, a promotion of a core electron (1σ, 2σ, or 3σ) to the 3π orbital forms a prominent absorption peak whereas a promotion of the core electron to 9σ forms a broad structure characteristic of a shape resonance due to a σ^* resonant state. 8σ is embedded in the Rydberg region close to the thresholds. It is worth noting that 8σ and 9σ have electron distributions similar to $5\sigma_g$ and $4\sigma_u$ in CO_2. The N_2O molecule has four vibrational modes, two stretching modes $(v_1',0,0)$ and $(0,0,v_3')$, and a doubly degenerate bending mode $(0,v_2',0)$. $(v_1',0,0)$ and $(0,0,v_3')$ are similar to symmetric and antisymmetric vibrations, respectively, in CO_2 and thus are often called quasisymmetric and quasiantisymmetric stretching vibrations, respectively. It is found that N_c $1s$ photoionization is predominately accompanied by excitation of the quasisymmetric stretching vibrations $(v_1',0,0)$, whereas N_t $1s$ photoionization is accompanied by excitation of both quasisymmetric $(v_1',0,0)$ and quasiantisymmetric $(0,0,v_3')$ stretching vibrations [19]. We report here measured and calculated fully vibrationally resolved partial cross sections and asymmetry parameters for N_c and N_t K-shell (i.e., 2σ and 3σ) photoionization of the N_2O molecule in the σ^* shape resonance regions. The comparison in v_1' dependence between the N_c $1s$ and N_t $1s$ photoionization, as well as the comparison between the v_1' and v_3' dependence in the N_t $1s$, photoionization is of particular interest.

II. EXPERIMENT

The experiments were carried out on the C branch of the soft x-ray photochemistry beam line 27SU [20,21] at SPring-8, the 8 GeV synchrotron radiation facility in Japan. The radiation source is a figure-8 undulator providing radiation linearly polarized either in the horizontal plane of the storage ring (1st, 2nd… order) or in the vertical plane perpendicular to it (0.5th, 1.5th… order) [22]. Angle-resolved electron emission measurements were performed by changing the undulator gap, without rotation of the electron analyzer. The electron spectroscopy apparatus consists of a hemispherical electron analyzer (Gammadata-Scienta SES2002), a gas cell, and a differentially pumped chamber as described elsewhere [23].

The transmission function of the analyzer was measured by observing the Ne $1s$ line at relevant kinetic energies. The degree of linear polarization was determined by observing Ne $2s$ and $2p$ photolines and confirmed to be greater than 0.98 with the present setting of the optics [24]. In the analysis we thus assume complete polarization at the photon energies employed. The photon flux was measured by a photocurrent on the refocusing mirror before the gas cell. The readout of the photon flux cannot be considered linear over the energy region 410–460 eV, hence ion yield spectra of argon was recorded in the relevant energy region and normalized to theoretical data [25,26]. The readout of the photonflux varied with 10% over the entire region compared to theoretical data. Once these corrections were included each angle-resolved photoelectron spectrum was fitted using the parameters from Ref. [19]. Spectra corrected for anisotropic electron emission were constructed by combining the 0° and 90° spectra measured at the same photon energy according to the following equation, which assumes 100% linear polarization: $I(54.7°)=I(0°)+2I(90°)$.

III. THEORY

The theoretical methods used here are similar to that used previously to study the vibrationally specific cross sections for valence ionization of N_2O [27]. The vibrationally specific core ionization cross sections were computed using the Chase adiabatic approximation [28]. Thus we have computed the fixed-nuclei dipole photoionization matrix elements on a grid of geometries of the molecules. The vibrationally specific cross sections were then obtained by an integral of the product of initial and final vibrational states with the geometry dependent dipole matrix elements. The fixed-nuclei photoionization calculations were performed using the mulitichannel Schwinger configuration interaction (MCSCI) method [29–31]. In this approach the bound states, i.e., the initial N electron state, and the final $N-1$ electron ionized states are represented by configuration interaction (CI) wave functions. The scattering state is then represented using a close-coupling wave function constructed from a sum of

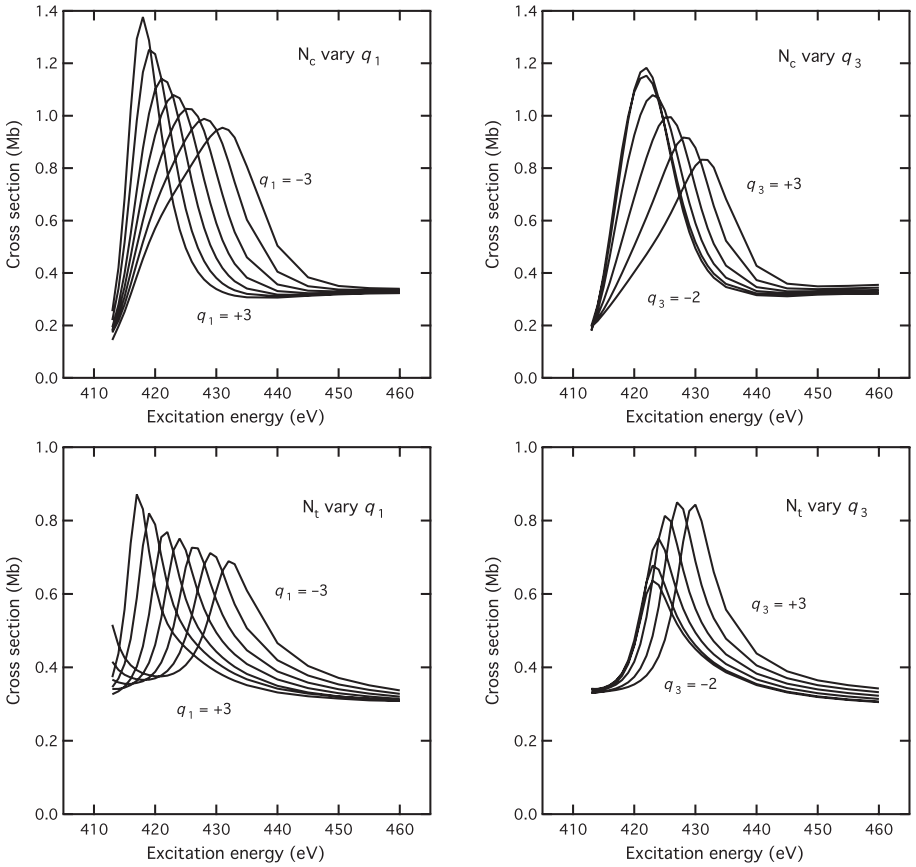

FIG. 1. Fixed-nuclei cross sections for N_c and N_t K-shell photoionization of N_2O. In each case the coordinate q_i that is not being varied is held constant with a value of 0, i.e., at the value at the equilibrium geometry of the ground state of N_2O.

products of ion states and one-electron channel continuum functions. The continuum functions are represented numerically using the single-center expansion (SCE) method.

For N_2O, the bound orbitals were computed using a complete active space self-consistent field (CASSCF) calculation on the ground state with eight σ orbitals and three sets of π orbitals. The active orbitals included five of the σ orbitals and all of the π orbitals. The CASSCF calculations were performed using the MOLPRO program [32].

For the scattering calculation, the initial state was constructed from the CASSCF orbitals using a small CI wave function. The CI wave function contained all excitations through quadrupole excitations, but only into the two virtual orbital sets obtained in the CASSCF calculations. In the CI calculation, all orbitals were active except the O 1*s* orbital. For the ion state, similar CI calculations were performed using the same initial state CASSCF orbitals. In the case of the ion states, only triple excitations were allowed into the virtual valence orbitals. This led to 2636 configuration state functions (CSFs) in the initial state calculation and 4516 CSFs in the ion state calculation. By an analysis of the CI wave functions, it was found that the N_t ion state corresponded to the 1797th eigenvector of the CI Hamiltonian in $^2\Sigma$ symmetry (including both Σ^+ and Σ^- states) and the N_c state was the 1798th eigenvector. In the CI calculation, where all integrals are evaluated using the SCE method, the computed ionization potentials (IPs) for the experimental equilibrium geometry of the ground state ($R_{N\text{-}N}$=1.1273 Å and $R_{N\text{-}O$=1.1851 Å [33]) was 414.7 eV for the N_t state and 421.3 eV for the N_c state. In all scattering calculations these IPs are adjusted to the experimental values of 408.44 eV and 412.46 eV for the N_t and N_c states, respectively [34].

The vibrational integrals were performed using a two-dimensional grid of linear geometries to describe the bond stretching motions neglecting the bending motion of the molecule. The geometries were sampled using the normal coordinates of the ground state using the experimental harmonic potential [33,35]. Thus the geometries are described using coordinates q_1 and q_3, where the bond lengths are defined as $R_{N\text{-}N}$=1.1273 Å+0.018 02 Å q_1−0.043 88 Å q_3 and $R_{N\text{-}O$=1.1851 Å+0.039 24 Å q_1+0.033 21 Å q_3. The corresponding harmonic frequencies are 161 meV for q_1 and 283 meV for q_3 [35]. Using these normal modes, we computed the fixed nuclei cross section on a rectangular grid where q_1 had the values −3, −2, −1, 0, 1, 2, 3, and q_3 had the values −2, −1, 0, 1, 2, 3. The main photoionization calculations were performed including both the N_t and N_c hole states. The single center expansion included up to l=100 for scattering wave functions and molecular orbitals.

The vibrational states used to obtain the vibrationally averaged dipole matrix elements were computed using the potentials obtained by Ehara *et al.* [19]. The potentials we used in the present study are the empirically optimized equivalent-core approximation (ECA) coupled-cluster singles and doubles with noniterative triples [CCSD(T)] potentials discussed in Ref. [19]. In these potentials, the equilibrium bond lengths have been slightly adjusted from their *ab initio* values to give agreement between theory and experiment for the main vibrational branching ratios at a photon energy of 450 eV. The ground state potential was shifted so that the

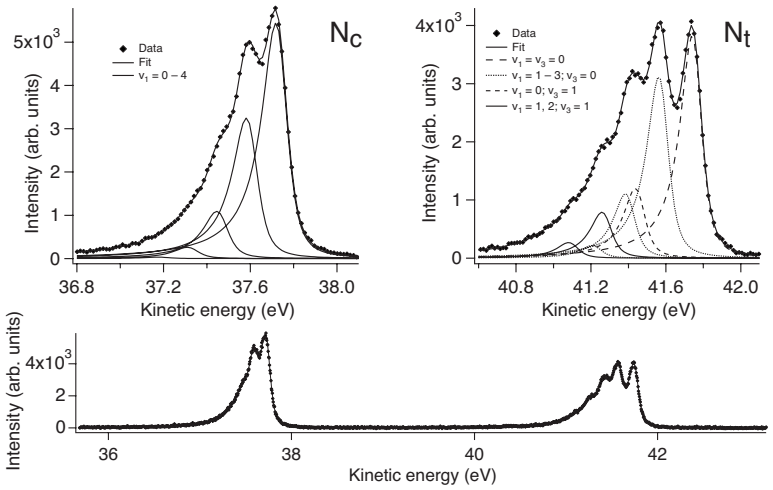

FIG. 2. *K*-shell photoelectron spectra of N_2O at a photon energy of 450 eV. The lower frame shows the region of the N_t and N_c ion states of N_2O^+. The upper frames show expanded views of the two spectra with the least squares fit of the profiles.

minimum occurred at the experimental equilibrium structure which has $R_{N\text{-}N}=1.1273$ Å and $R_{N\text{-}O}=1.1851$ Å [33]. In the N_t ion state the equilibrium geometry then was $R_{N\text{-}N}=1.1205$ Å and $R_{N\text{-}O}=1.1190$ Å, and in the N_c ion state the equilibrium geometry was $R_{N\text{-}N}=1.1398$ Å and $R_{N\text{-}O}=1.2336$ Å. In terms of the ground state normal modes discussed above, the equilibrium geometry of the N_c core ionized state had $q_1=1.096$ and $q_3=0.165$ and the N_t core ionized state had $q_1=-1.347$ and $q_3=-0.398$.

The vibrational wave functions were expanded in a direct product basis set of harmonic oscillator states obtained from a harmonic approximation to the computed potentials. This basis set consisted of states up to $\nu=10$ in each normal mode. We note the potential energy surface for the N_c state is dissociative with a computed barrier to dissociation of ~0.80 eV [19]. The low-lying states in the N_c well are below this barrier and would only slowly dissociate through tunneling. Using the restricted basis set expansion, which is localized in the bound part of the potential, the effects of this dissociative process are neglected.

In the adiabatic approximation used here, the cross sections are computed within the fixed-nuclei approximation on a grid of geometries. In Fig. 1 the cross sections for some of those geometries are shown.

IV. RESULTS AND DISCUSSION

A. General features

Figure 2 shows the N_c *K*-shell photoelectron spectra of N_2O measured at a photon energy of ~450 eV, i.e., 41.6 eV above the N_t *K*-shell ionization threshold and 37.5 eV above the N_c threshold [34]. These spectra have been normalized for the photon flux and gas pressure and corrected for the transmission function. Each partial cross section was determined from the intensity of the individual components in the angle-resolved spectra. The effect of postcollision interaction (PCI) was included by simulating the individual profiles with the equation of van der Straten [36]. The PCI profile was convoluted with a Gaussian with full width at half maximum of ~45 meV to account for instrumental broadening. In the fitting, the natural width [118(2) meV] and vibrational frequencies [N_c $\omega_1=136(2)$ meV, N_t $\omega_1=178(1)$ meV, N_t $\omega_3=303(2)$ meV] were fixed to the values obtained in Ref. [19].

The total cross sections for N_c and N_t are shown in Fig. 3 together with the corresponding asymmetry parameters. The present measurements (closed symbols) reasonably agree with the previous, vibrationally unresolved measurements (open symbols) of Schmidbauer *et al.* [37]. The absolute scale for the cross section in Fig. 3 (and also in Figs. 4 and 6

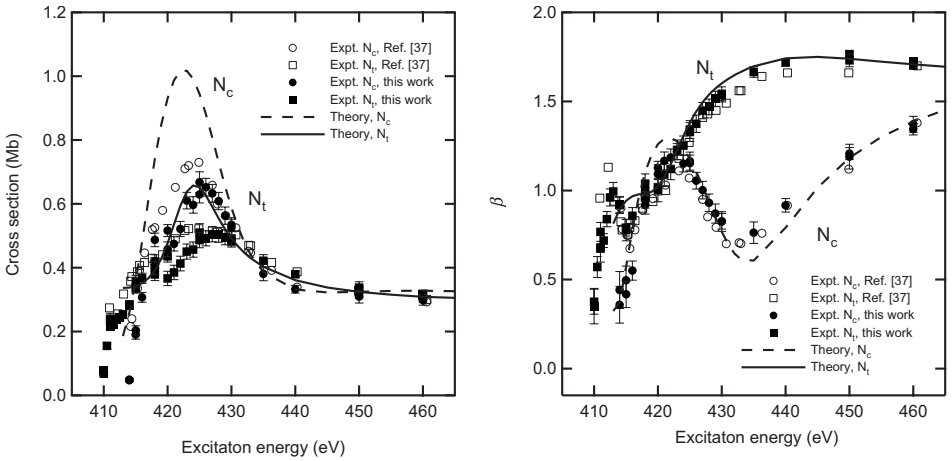

FIG. 3. Total *K*-shell photoionization cross sections and photoelectron asymmetry parameters for ionization leading to the N_c and N_t states of N_2O. Calculated results for the N_t ionization (solid line) and N_c ionization (dashed line) are compared to the present experimental results (solid squares for N_t and solid circles for N_c and to the data of Schmidbauer *et al.* [37]) given as the corresponding open symbols.

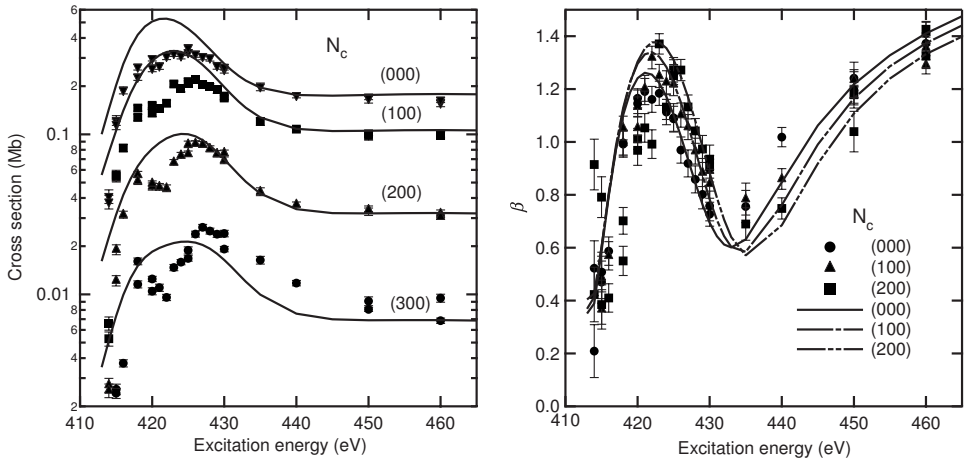

FIG. 4. Vibrationally resolved cross sections $\sigma_{(v_1',0,0)}$ $(v_1'=0-3)$ and photoelectron asymmetry parameters $\beta_{(v_1',0,0)}$ $(v_1'=0-2)$ for N_c K-shell photoionization of N_2O.

shown later) is based on the vibrationally unresolved measurements of Schmidbauer *et al.*, where we have multiplied the results of the earlier data by 0.6 to account for the high energy spectroscopic factors as suggested by the authors [37]. The present measurement only provides the relative scale and is normalized to the result of Schmidbauer *et al.* for N_c at the photon energy ~450 eV. The cross sections both for N_c and N_t exhibit shape resonances. The agreement between theory and experiment is reasonable, although the computed results show a more pronounced enhancement in region of the shape resonance than is seen in the experiment.

The vibrationally averaged asymmetry parameter $\beta_{N_c} \equiv \Sigma_{v_1'}\beta_{v_1'}\sigma_{v_1'}/\Sigma_{v_1'}\sigma_{v_1'}$ is shown in the right panel of Fig. 3. The present measurements (closed circles) agree well with the previous, vibrationally unresolved measurements (open circles) of Schmidbauer *et al.* [37]. The asymmetry parameters both for N_c and N_t exhibit the shape resonance effects, though the effects appear differently: the asymmetry parameter exhibits dispersive behavior for N_c and the monotonic rapid decrease for N_t in the region of the shape resonance. The agreement between theory and experiment is reasonable.

B. Vibrationally resolved N_c 1*s* photoionization

The spectral dependence of the measured N_c K-shell photoionization cross sections $\sigma_{v_1'}$ for $v_1'=0-3$ is shown in Fig. 4 together with theoretical predictions. The σ^* shape resonance is clearly seen in the spectral dependence of $\sigma_{v_1'}$. As seen in Fig. 4, the observed shape resonance peak moves up from ~420 eV to ~425 eV as v_1' goes from 0 to 3 in agreement with the theoretical predictions. The computed asymmetry parameters also show the same v_1'-dependent resonant feature that is seen in the experiment.

In the Franck-Condon approximation, the vibrational branching ratios are independent of the photon energy. The variation of the cross sections with v_1' seen in Fig. 4, however, leads to non-Franck-Condon behavior of the vibrational branching ratios [38]. The experimental and computed vibrational branching ratios, $\sigma_{(v_1',0,0)}/\sigma_{(0,0,0)}$, are plotted in Fig. 5. Although the magnitude of the resonance features in the cross sections is larger than in the experiment, there is good agreement for the relative enhancement for each vibrational state. It would thus appear that the source of the discrepancies between the calculated and measured cross sections must have a similar relative effect on the cross sections for ionization to the different ion vibrational states.

The upward shift of the σ^* shape resonance with increasing v_1' originates from the fact that the shape resonance peak in the N_c 1*s* cross section for a fixed-nuclei geometry in Fig. 1 shows upward shift in a monotonic manner when the quasisymmetric stretch q_1 is decreased. The relation between the fixed-nuclei cross section and v_1'-dependent cross section can be well understood by introducing the characteristic v_1' dependent displacement defined as $\langle v_1'|q_1|0\rangle/\langle v_1'|0\rangle$, where $|0\rangle$ and $|v_1'\rangle$ are vibrational wave functions of the neutral ground

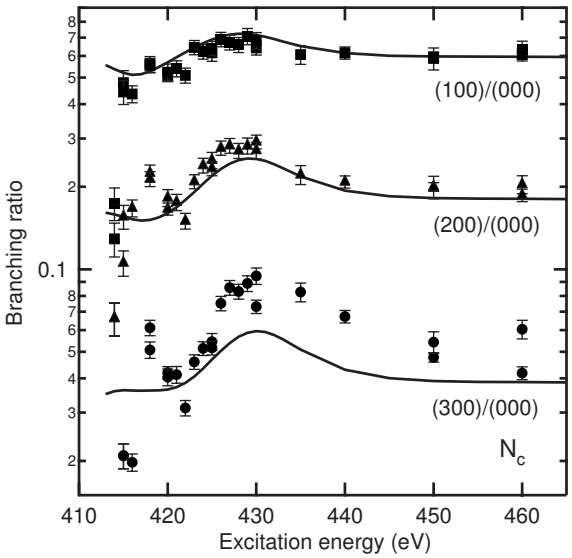

FIG. 5. Measured and computed vibrational branching ratios, $\sigma_{(v_1',0,0)}/\sigma_{(0,0,0)}$ $(v_1'=1-3)$, for ionization in N_c K-shell photoionization of N_2O.

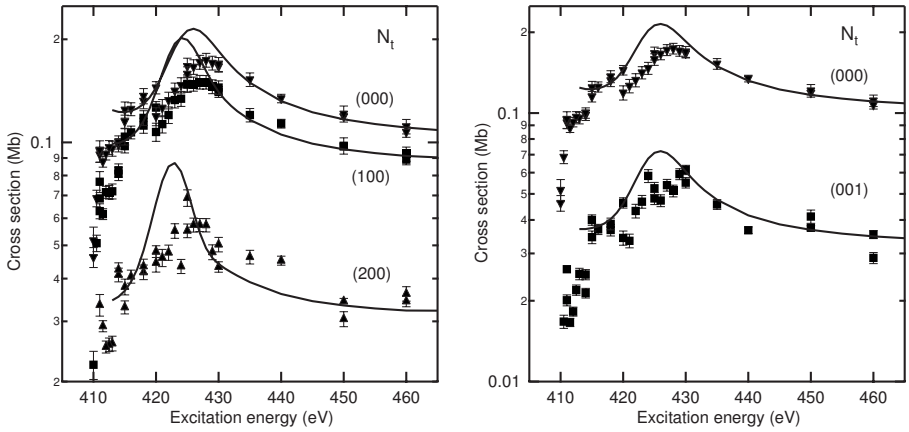

FIG. 6. Vibrationally resolved cross sections $\sigma_{(v_1',0,0)}$ $(v_1'=0-3)$ and $\sigma_{(0,0,v_3')}$ $(v_3'=0-2)$ for N_t K-shell photoionization of N_2O.

state and core ionized state, respectively [6,9,13].

A similar v'-dependent shape resonance behavior was observed in the O 1s photoionization of CO. In that case, the equilibrium bond distance of the O 1s ionized CO, R_e^+, is longer than that of the neutral ground state R_e^+, $R_e^+ - R_e^0 > 0$, and thus the characteristic bond length, $R_e^0 + \langle v'|\delta R|0\rangle / \langle v'|0\rangle$, decreases with increasing the vibrational quantum number v' of the O 1s ionized state. In analog to the O 1s photoionization of CO, the upward shift of the shape resonance energy in the N_c 1s photoionization, with increasing v_1', can be attributed to the shortening of both the characteristic N-N and N-O bond lengths with increasing v_1', which in turn indicates that the equilibrium N-N and N-O bond lengths in the N_c 1s-ionized state are both longer than those in the neutral ground state. This result is consistent with the value of $q_1=1.096$ found for the structure of the N_c state in the optimized ECA CCSD(T) potential.

The right-hand part of Fig. 4 shows the measured asymmetry parameters $\beta_{v_1'}$ for $v_1=0-2$ as a function of energy. The σ^* shape resonance is responsible for the characteristic photon energy dependence of $\beta_{v_1'}$. The maximum in $\beta_{v_1'}$ appears close to the shape resonance energy, i.e., at 420 eV for $\beta_{v_1'=0}$ and moves toward higher excitation energies with increasing v_1'. The calculated asymmetry parameters $\beta_{v_1'}$ are also shown in Fig. 4, where they are seen to reproduce the measurements quite well.

C. Vibrationally resolved N_t 1s photoionization

The vibrationally resolved N_t 1s photoionization cross sections are shown in Fig. 6. Here we again see a significant degree of excitation of the quasisymmetric mode v_1'. However, as seen in the right-hand panel of Fig. 6, there is also a significant degree of excitation of the quasiantisymmetric mode v_3'. The agreement between theory and experiment is quite good, except for energies just below the peak in the theoretical results. Additionally, the experimental cross sections show a sharp drop just above threshold that is not seen in the calculations. The peak in the cross section shifts to lower excitation energy as v_1' increases in both theory and experiment.

This effect can be more clearly seen in the line shapes of the branching ratios shown in Fig. 7. In both the (100)/(000) and (200)/(000) branching ratios there is a maximum at low energy and a minimum at higher energy indicating that the peak in the cross section has shifted to lower energy for the higher vibrational excitation levels relative to the ground state of the ion. In the vibrational resolved cross sections leading to the (001) state there is only a very weak non-Franck-Condon vibrational effect in the region of the resonance as can be seen by the nearly constant branching ratios shown in Fig. 7. Again, both in the cross section and in the branching ratios, the results of the present calculations near threshold do not agree with the experimental results.

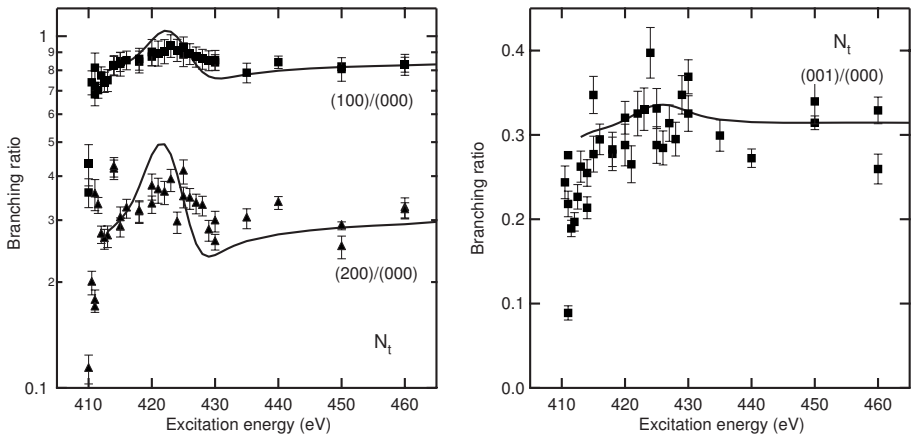

FIG. 7. Measured and computed vibrational branching ratios, $\sigma_{(v_1',0,0)}/\sigma_{(0,0,0)}$ $(v_1'=1-3)$ and $\sigma_{(0,0,v_3')}/\sigma_{(0,0,0)}$ $(v_3'=1,2)$, for ionization in N_t K-shell photoionization of N_2O.

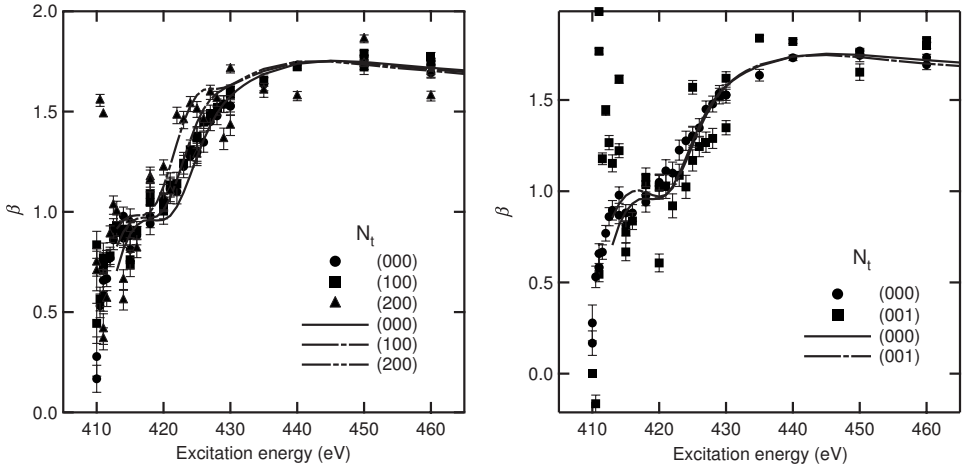

FIG. 8. Vibrationally resolved asymmetry parameters $\beta_{(v_1',0,0)}$ $(v_1'=0-3)$ and $\beta_{(0,0,v_3')}$ $(v_3'=0-2)$ for N_t K-shell photoionization of N_2O.

The fact that the peak in the resonance position in the N_t $1s$ ionization shifts to lower energy with increasing v_1' is very much analogous to the shift to lower energy seen in the C $1s$ ionized states of CO [6]. This is consistent with the computed structure of the ion state which has a significant contraction in the length of the molecule, with $q_1=-1.347$, in an analogous fashion to the contraction in the CO bond length in the C $1s$ ionized state of CO.

The fact that the N_t $1s$ ionization does involve some excitation of the quasiantisymmetric mode q_3 where the N_c $1s$ ionization does not, is also consistent with the significantly larger shift in $q_3=-0.398$ for the N_t equilibrium geometry compared to the $q_3=0.165$ for the N_c state. As seen in Fig. 1, variation of the fixed nuclei cross section by the variation of the quasiantisymmetric stretch q_3 shows a behavior somewhat different from that of q_1. In a triatomic molecule with a center of symmetry, e.g., CO_2, the cross section at $+q_3$ and $-q_3$ would be the same. In N_2O, there is a tendency for the cross section turn around as a function of q_3 at negative values, however, not to the extent that would be found in a system with a center of symmetry. Both the measurement and theory show rather weak v_3' dependence of the shape resonance energy due to this characteristic q_3-dependent behavior of the fixed nuclei cross section.

The vibrationally resolved photoelectron asymmetry parameters for N_t $1s$ ionization are shown in Fig. 8. Here we see small shifts of the curves to lower energy as the v_1' and v_3' are increased. With the exception of the near threshold region the computed values are generally in very good agreement with experiment.

V. CONCLUSIONS

The vibrationally specific cross sections and photoelectron asymmetry parameters have been measured for N_c and N_t ionization of N_2O. One qualitative feature which has been analyzed is the shift in the position of the σ^* as a function of the vibrational state that is excited. In the case of the N_c ionization, increasing excitation of the v_1' quasisymmetric mode leads to a shift of the resonance to higher energy. In contrast, in the N_t ionization, increasing v_1' leads to a shift of the resonance position to lower energy. These results are consistent with the computed equilibrium structures of the two ion states which has the N_c structure shifted to longer bond lengths and the N_t structure shifted to shorter bond lengths relative to the N_2O ground state [19].

The corresponding cross section computed using the MCSCI method are in reasonably good agreement with the measured data. This is seen in particular for the relative quantities: branching ratios and photoelectron asymmetry parameters. There are a number of limitations of the present calculations which might be the cause of the discrepancies with the experiments. First the bending vibrational modes have been ignored. These modes are not found to be excited in the experimental data; however, in the calculation one should still average over that motion which would tend to reduce the magnitudes of the resonant features. The features seen at low energy in the experiment may be due to autoionization resonance states which can be expected below the thresholds of shake-up states that should occur above the $1s$ thresholds. Such states are not included in the present two-channel calculations.

ACKNOWLEDGMENTS

The experiment was carried out with the approval of the SPring-8 program review committee. This study was supported by Grants-in-Aid for Scientific Research from the Japanese Society for the Promotion of Science (JSPS) and by the Chemical Sciences, Geosciences and Biosciences Division, Office of Basic Energy Sciences, Office of Science, U.S. Department of Energy. R.R.L. acknowledges JSPS for financial support and Tohoku University for hospitality during his stay there. J.S. acknowledges Tohoku University for hospitality and financial support during his stay.

[1] J. L. Dehmer, D. Dill, and A. C. Parr, in *Photophysics and Photochemistry in the Vacuum Ultraviolet*, edited by S. McGlynn, G. Findly, and R. Huebner (Reidel, Dordrecht, 1985), p. 341.
[2] J. L. Dehmer, D. Dill, and S. Wallace, Phys. Rev. Lett. **43**, 1005 (1979).
[3] K. J. Randall, A. L. D. Kilcoyne, H. M. Köppe, J. Feldhaus, A. M. Bradshaw, J.-E. Rubensson, W. Eberhardt, Z. Xu, P. D. Johnson, and Y. Ma, Phys. Rev. Lett. **71**, 1156 (1993).
[4] H. M. Koppe, B. Kempgens, A. L. D. Kilcoyne, J. Feldhaus, and A. M. Bradshaw, Chem. Phys. Lett. **260**, 223 (1996).
[5] M. N. Piancastelli, J. Electron Spectrosc. Relat. Phenom. **100**, 167 (1999), and references therein.
[6] D. A. Mistrov, A. De Fanis, M. Kitajima, M. Hoshino, H. Shindo, T. Tanaka, Y. Tamenori, H. Tanaka, A. A. Pavlychev, and K. Ueda, Phys. Rev. A **68**, 022508 (2003).
[7] S. K. Semenov, N. A. Cherepkov, A. De Fanis, Y. Tamenori, M. Kitajima, H. Tanaka, and K. Ueda, Phys. Rev. A **70**, 052504 (2004).
[8] U. Hergenhahn, J. Phys. B **37**, R89 (2004), and references therein.
[9] A. De Fanis, D. A. Mistrov, M. Kitajima, M. Hoshino, H. Shindo, T. Tanaka, H. Tanaka, Y. Tamenori, A. A. Pavlychev, and K. Ueda, Phys. Rev. A **71**, 052510 (2005).
[10] S. K. Semenov, N. A. Cherepkov, M. Matsumoto, K. Fujiwara, E. Kukk, H. Yoshida, T. Tanaka, M. Kitajima, H. Tanaka, A. De Fanis, and K. Ueda, J. Phys. B **39**, 375 (2006).
[11] M. Hoshino, K. Nakagawa, C. Makochekanwa, T. Tanaka, N. Kuze, M. Matsumoto, K. Fujiwara, A. De Fanis, Y. Tamenori, M. Kitajima, H. Tanaka, and K. Ueda, Chem. Phys. Lett. **421**, 256 (2006).
[12] M. Hoshino, K. Nakagawa, T. Tanaka, M. Kitajima, H. Tanaka, A. De Fanis, K. Wang, B. Zimmermann, V. McKoy, and K. Ueda, J. Phys. B **39**, 3047 (2006).
[13] M. Hoshino, K. Nakagawa, T. Tanaka, M. Kitajima, H. Tanaka, A. De Fanis, X. O. Brykalova, D. A. Mistrov, A. A. Pavlychev, T. Hatamoto, and K. Ueda, J. Phys. B **39**, 3655 (2006).
[14] A. Kivimäki, B. Kempgens, K. Maier, H. M. Köppe, M. N. Piancastelli, M. Neeb, and A. M. Bradshaw, Phys. Rev. Lett. **79**, 998 (1997).
[15] W. Domcke and L. S. Cederbaum, Chem. Phys. **25**, 189 (1977).
[16] K. Maier, A. Kivimaki, B. Kempgens, U. Hergenhahn, M. Neeb, A. Rudel, M. N. Piancastelli, and A. M. Bradshaw, Phys. Rev. A **58**, 3654 (1998).
[17] N. V. Dobrodey, H. Koppel, and L. S. Cederbaum, Phys. Rev. A **60**, 1988 (1999).
[18] J. Murakami, M. C. Nelson, S. L. Anderson, and D. M. Hanson, J. Chem. Phys. **85**, 5755 (1986).
[19] M. Ehara, R. Tamaki, H. Nakatsuji, R. R. Lucchese, J. Söderström, T. Tanaka, M. Hoshino, M. Kitajima, H. Tanaka, A. De Fanis, and K. Ueda, Chem. Phys. Lett. **438**, 14 (2007).
[20] H. Ohashi, E. Ishiguro, Y. Tamenori, H. Kishimoto, M. Tanaka, M. Irie, T. Tanaka, and T. Ishikawa, Nucl. Instrum. Methods Phys. Res. A **467-468**, 529 (2001).
[21] H. Ohashi, E. Ishiguro, Y. Tamenori, H. Okumura, A. Hiraya, H. Yoshida, Y. Senba, K. Okada, N. Saito, I. H. Suzuki, K. Ueda, T. Ibuki, S. Nagaoka, I. Koyano, and T. Ishikawa, Nucl. Instrum. Methods Phys. Res. A **467-468**, 533 (2001).
[22] T. Tanaka and H. Kitamura, J. Synchrotron Radiat. **3**, 47 (1996).
[23] Y. Shimizu, H. Ohashi, Y. Tamenori, Y. Muramatsu, H. Yoshida, K. Okada, N. Saito, H. Tanaka, I. Koyano, S. Shin, and K. Ueda, J. Electron Spectrosc. Relat. Phenom. **114-116**, 63 (2001).
[24] H. Yoshida, Y. Senba, M. Morita, T. Goya, A. De Fanis, N. Saito, K. Ueda, Y. Tamenori, and H. Ohashi, in *Synchrotron Radiation Instrumentation: Eighth International Conference on Synchrotron Radiation Instrumentation*, San Francisco, CA, 2003, edited by T. Warwick, AIP Conf. Proc. No. 705 (AIP, Melville, NY, 2004), p. 267.
[25] G. V. Marr and J. B. West, At. Data Nucl. Data Tables **18**, 497 (1976).
[26] R. F. Reilman and S. T. Manson, Astrophys. J., Suppl. **40**, 815 (1979).
[27] G. J. Rathbone, E. D. Poliakoff, J. D. Bozek, D. Toffoli, and R. R. Lucchese, J. Chem. Phys. **123**, 014307 (2005).
[28] D. M. Chase, Phys. Rev. **104**, 838 (1956).
[29] R. R. Lucchese, K. Takatsuka, and V. McKoy, Phys. Rep. **131**, 147 (1986).
[30] R. E. Stratmann and R. R. Lucchese, J. Chem. Phys. **102**, 8493 (1995).
[31] R. E. Stratmann, R. W. Zurales, and R. R. Lucchese, J. Chem. Phys. **104**, 8989 (1996).
[32] H.-J. Werner, P. J. Knowles, R. Lindh, M. Schutz, P. Celani, T. Korona, F. R. Manby, G. Rauhut, R. D. Amos, A. Bernhardsson, A. Berning, D. L. Cooper, M. J. O. Deegan, A. J. Dobbyn, F. Eckert, C. Hampel, G. Hetzer, A. W. Lloyd, S. J. McNicholas, W. Meyer, M. E. Mura, A. Nicklass, P. Palmieri, R. Pitzer, U. Schumann, H. Stoll, A. J. Stone, R. Tarroni, and T. Thorsteinsson, MOLPRO, Version 2006.1, a package of *ab initio* computer programs, Cardiff, UK, 2006.
[33] J.-L. Teffo and A. Chedin, J. Mol. Spectrosc. **135**, 389 (1989).
[34] M. Alagia, R. Richter, S. Stranges, M. Agaker, M. Strom, J. Söderström, C. Sathe, R. Feifel, S. Sorensen, A. De Fanis, K. Ueda, R. Fink, and J.-E. Rubensson, Phys. Rev. A **71**, 012506 (2005).
[35] J. M. L. Martin, P. R. Taylor, and T. Lee, Chem. Phys. Lett. **205**, 535 (1993).
[36] P. van der Straten, R. Morgenstern, and A. Niehaus, Z. Phys. D: At., Mol. Clusters **8**, 35 (1988).
[37] M. Schimidbauer, A. L. D. Kilcoyne, K. J. Randall, J. Feldhaus, A. M. Bradshaw, M. Braunstein, and V. McKoy, J. Chem. Phys. **94**, 5299 (1991).
[38] E. D. Poliakoff and R. R. Lucchese, Phys. Scr. **74**, C71 (2006).